

Orbital Angular Momenta and Geometric Phase Characteristics of Spin-polarized Components of a General Paraxial Beam-field

Anirban Debnath* and Nirmal K. Viswanathan†
School of Physics, University of Hyderabad, Hyderabad 500046, India
(Dated: June 28, 2022)

We explore a subtle and fundamental nature of spin-orbit interaction (SOI) in a general paraxial beam-field by mathematically characterizing the orbital angular momentum (OAM) flux densities of the spin-polarized component fields via Barnett's flux determination formalism. We show the application of our formalism by considering the special case of a Brewster-reflected paraxial beam, for which we explore specific details such as non-canonical vortex phase structures and single-photon interpretation of the field function. The phases of the spin-component fields are interpreted as geometric phases; and we devise an experimental method of direct measurement of these phases by transferring the spatial phase information to the polarization domain — thus demonstrating a classical analog von Neumann measurement. Our complete mathematical characterization of SOI and its relevance to the direct measurement of geometric phase can find potential application in future methods exploring OAM and geometric phase characteristics in other general optical systems.

CONTENTS

I. Introduction	1
II. Formalism	2
III. Case Study : Spin-Orbit Interaction in a Brewster-reflected Paraxial Beam	3
IV. Geometric Phase Characteristics	5
A. Interpretation	5
B. Experimental Measurement of Geometric Phase	5
C. Comments on Beam-shifts and Spin-shifts	7
V. Conclusion	7
Acknowledgments	8
References	8

I. INTRODUCTION

More than a century ago, the angular momentum (AM) of light was first identified by Poynting in the form of spin angular momentum (SAM), associated to circular polarizations [1]. This phenomenon was subsequently verified experimentally by Beth [2]. Decades later, Allen, Beijersbergen, Spreeuw and Woerdman identified the

presence of orbital angular momentum (OAM) of light in Laguerre-Gaussian (LG) laser modes [3]. Since then, the literature has been substantially enriched by many researchers via fundamentally significant theoretical understanding on the subject as well as via ingenious experimental works [4–37].

In the present paper, we aim to explore the SAM and OAM characteristics of a paraxial beam-field in a specific way. The general cross-sectional field \mathcal{E} of a paraxial beam, propagating along $\hat{\mathbf{z}}$, can be expressed (by neglecting divergence/convergence and the $\hat{\mathbf{z}}$ component of the field) as the sum of its linearly polarized component fields $\mathcal{E}_x \hat{\mathbf{x}}$ and $\mathcal{E}_y \hat{\mathbf{y}}$; or as the sum of its spin-polarized component fields $\mathcal{E}_+ \hat{\sigma}^+$ and $\mathcal{E}_- \hat{\sigma}^-$; or, in general, as the sum of any pair of orthogonally polarized component fields. The spin-polarized fields $\mathcal{E}_\pm \hat{\sigma}^\pm$ carry spin angular momentum (SAM) $\pm\hbar$ per photon; whereas, the general complex forms of the component fields \mathcal{E}_x , \mathcal{E}_y , \mathcal{E}_+ , \mathcal{E}_- etc. with variable phase structures are associated to orbital angular momentum (OAM). Hence, the complete field structure — which is a single construct containing a coupling between spin characteristics and orbital characteristics — contains an interplay between SAM and OAM, giving rise to significant phenomena that cannot be realized by only SAM or only OAM individually. This coupling or interplay is known as the spin-orbit interaction (SOI). The SOI phenomena in paraxial as well as non-paraxial beam-fields have been extensively studied in the literature [3, 4, 7, 16, 25, 27–31, 33, 34, 36]. The association of OAM with variable phase structures — especially with vortex phases — are well understood and experimentally verified [14, 15, 32, 36–39]. The relation of SOI with Goos-Hänchen (GH) shift, Imbert-Fedorov (IF) shift and spin shifts (including spin Hall effect of light, SHEL) is rigorously analyzed and well-established

* anirban.debnath090@gmail.com

† nirmalsp@uohyd.ac.in

[4, 27–31, 40–63].

However, identification of the variable phase structure is not sufficient to completely characterize the OAM; and we emphasize on an exact calculation of the associated OAM to achieve a complete mathematical characterization of SOI in a beam-field. This is especially important in the case of vortex phases, because a phase vortex of topological charge t (which is distinguished from the order l of an LG mode) does not generally imply an OAM $t\hbar$ per photon [16, 36]. In the present paper, we use Barnett's SAM and OAM flux calculation method [25] to derive a general expression of the OAM flux densities of the spin-polarized component fields $\mathcal{E}_\pm \hat{\sigma}^\pm$ of a general paraxial beam-field. We then verify that these individual OAM flux densities add up to give the OAM flux density of the complete beam-field — implying that the OAM of the total field is consistently distributed between the spin-component fields, with AM conservation satisfied. This distribution is a subtle and unique nature of SOI taking place in a general paraxial beam-field — which we interpret in this paper.

Subsequently, we present a case study involving Brewster reflection of a paraxial beam, whose total SAM and OAM are zero, but the spin-polarized component fields carry OAM of equal magnitudes and opposite signs — consistent with our interpretation. We explore the non-canonical nature [36] of the associated phase vortices; and establish a consistent single-photon interpretation of the beam-field function.

The variable phase structures of the component fields can be interpreted as geometric phases, which are responsible for SOI [33]. We show that SOI in the considered general form of the beam-field enables (via appropriate field-transformations) the transfer of the geometric phase information (which is in the spatial domain) to the polarization domain — by virtue of which the information can be extracted via Stokes parameter measurements. This method thus represents a classical analog von Neumann measurement [64], by considering the spatial functions as the measurand system states and the polarization states as the measuring device states. We verify this method of geometric phase measurement via simulation and experiment.

In this way, our OAM flux calculation leads to a complete mathematical characterization of SOI by exploring subtle and fundamental details of the beam-field; whereas, the implementation of our geometric phase measurement method indicates towards the possibility of creating other future methods utilizing SOI for the transfer of orbital information to spin/polarization domain, enabling convenient ways of extracting the relevant information.

II. FORMALISM

We consider the general cross-sectional field

$$\mathcal{E} = \mathcal{E}_x \hat{\mathbf{x}} + \mathcal{E}_y \hat{\mathbf{y}} \quad (1)$$

of a paraxial beam, propagating along $\hat{\mathbf{z}}$ (\mathcal{E}_x and \mathcal{E}_y are complex in general). The SAM and OAM flux density functions for this field across a beam cross-sectional area is given by [25, 37]

$$M_{spin} = \frac{\epsilon_0}{2k} \Im(\mathcal{E}_x^* \mathcal{E}_y - \mathcal{E}_y^* \mathcal{E}_x); \quad (2)$$

$$M_{orb} = \frac{\epsilon_0}{2k} \Im[(\partial_\phi \mathcal{E}_x) \mathcal{E}_x^* + (\partial_\phi \mathcal{E}_y) \mathcal{E}_y^*]; \quad (3)$$

where, ϵ_0 is the permittivity of empty space; k is the wavevector magnitude $2\pi/\lambda$; $\Im(Z)$ denotes the imaginary part of a complex quantity Z ; and $\partial_\phi = x\partial_y - y\partial_x$ denotes partial differentiation with respect to the azimuthal coordinate variable ϕ . The total SAM and OAM transferred across the entire beam cross-section per unit time are then obtained as

$$L_{spin} = \int_{-\infty}^{\infty} \int_{-\infty}^{\infty} M_{spin} dx dy; \quad L_{orb} = \int_{-\infty}^{\infty} \int_{-\infty}^{\infty} M_{orb} dx dy. \quad (4)$$

While the total fluxes L_{spin} and L_{orb} are the desired physically relevant quantities, a straightforward physical interpretation of the flux densities M_{spin} and M_{orb} are to be made with caution — because, any function M , satisfying

$$\int_{-\infty}^{\infty} \int_{-\infty}^{\infty} M dx dy = 0, \quad (5)$$

can be added to M_{spin} and M_{orb} , without altering the physically relevant L_{spin} and L_{orb} results [25, 37].

We now emphasize on finding the OAM fluxes of the individual $\hat{\sigma}^\pm$ spin-component fields for a detailed characterization of the SOI phenomena in the beam-field. By writing $\hat{\mathbf{x}} = (\hat{\sigma}^+ + \hat{\sigma}^-)/\sqrt{2}$ and $\hat{\mathbf{y}} = (\hat{\sigma}^+ - \hat{\sigma}^-)/\sqrt{2}i$, we re-express the total beam-field \mathcal{E} [Eq. (1)] in terms of the $\hat{\sigma}^\pm$ spin-polarized component fields as

$$\mathcal{E} = \mathcal{E}_+ + \mathcal{E}_- = \mathcal{E}_+ \hat{\sigma}^+ + \mathcal{E}_- \hat{\sigma}^-; \quad \mathcal{E}_\pm = (\mathcal{E}_x \mp i\mathcal{E}_y)/\sqrt{2}. \quad (6)$$

The above complex forms of \mathcal{E}_\pm indicate towards variable phase structures in general — associated to individual OAM of the spin-component fields $\mathcal{E}_\pm = \mathcal{E}_\pm \hat{\sigma}^\pm$. To find these individual OAM, we express the fields \mathcal{E}_\pm in terms of $\hat{\mathbf{x}}$ and $\hat{\mathbf{y}}$ components as

$$\mathcal{E}_\pm = \mathcal{E}_{\pm x} \hat{\mathbf{x}} + \mathcal{E}_{\pm y} \hat{\mathbf{y}}; \quad \mathcal{E}_{\pm x} = \mathcal{E}_\pm/\sqrt{2}, \quad \mathcal{E}_{\pm y} = \pm i\mathcal{E}_\pm/\sqrt{2}. \quad (7)$$

Then, by replacing $\mathcal{E}_x \rightarrow \mathcal{E}_{\pm x}$ and $\mathcal{E}_y \rightarrow \mathcal{E}_{\pm y}$ in Eqs. (2) and (3), we find the SAM and OAM flux densities of the individual \mathcal{E}_\pm fields as

$$M_{spin}^\pm = \pm \frac{\epsilon_0}{2k} |\mathcal{E}_\pm|^2; \quad M_{orb}^\pm = \frac{\epsilon_0}{2k} \Im[\mathcal{E}_\pm^* (\partial_\phi \mathcal{E}_\pm)]. \quad (8)$$

The corresponding individual SAM and OAM fluxes through the entire beam cross-section are then obtained as

$$L_{spin}^\pm = \int_{-\infty}^{\infty} \int_{-\infty}^{\infty} M_{spin}^\pm dx dy; \quad L_{orb}^\pm = \int_{-\infty}^{\infty} \int_{-\infty}^{\infty} M_{orb}^\pm dx dy. \quad (9)$$

Even though a straightforward physical interpretation of M_{spin} is to be restricted in general considering the case of Eq. (5), the above form of M_{spin}^{\pm} [Eq. (8)] can be appropriately interpreted with physical consistency. The intensity of the fields \mathcal{E}_{\pm} are given by $I_{\pm} = (1/2\mu_0c)|\mathcal{E}_{\pm}|^2$; where, μ_0 is the magnetic permeability of empty space; and c is the speed of light in empty space. Considering an energy $\hbar\omega$ per photon ($\omega = ck$), we find the number of $\hat{\sigma}^{\pm}$ spin-polarized photons passing through a unit area of the beam cross-section per unit time as $n_{\pm} = I_{\pm}/\hbar\omega$. The SAM per photon, corresponding to \mathcal{E}_{\pm} , are then obtained as

$$l_{spin}^{\pm} = M_{spin}^{\pm}/n_{\pm} = \pm\hbar; \quad (10)$$

which is the expected physically significant result, since the \mathcal{E}_{\pm} fields are purely $\hat{\sigma}^{\pm}$ spin-polarized.

While the M_{spin}^{\pm} flux densities clearly associate $\pm\hbar$ SAM per photon to $\hat{\sigma}^{\pm}$ spin-polarizations, the general form of M_{orb}^{\pm} [Eq. (8)] requires elaborate case-specific analysis for further exploration. However, the nature of SOI in the present context can be readily interpreted. It is easily verified by using Eqs. (3), (6) and (8) that

$$M_{orb}^{+} + M_{orb}^{-} = M_{orb}; \quad (11)$$

which, via Eqs. (4) and (9), gives

$$L_{orb}^{+} + L_{orb}^{-} = L_{orb}. \quad (12)$$

The OAM flux L_{orb} of the total beam-field is thus distributed between the $\hat{\sigma}^{\pm}$ spin-polarized component fields as L_{orb}^{\pm} . This distribution of OAM between the spin-component fields is the true nature of SOI in a paraxial beam-field — as interpreted from the above result. Since Eq. (1) represents a general field, this interpretation is applicable to any general paraxial beam-field. The OAM remains separately conserved in this distribution process in addition to the total AM conservation, as understood from Eq. (12).

The above process of determination of the OAM fluxes L_{orb}^{\pm} and the interpretation on their consistent distribution between the spin-component fields are two central contents of the present paper. Clearly, an in-depth exploration of the individual L_{orb}^{\pm} terms is an integral part of understanding of this SOI phenomenon — especially in the cases where $L_{orb}^{-} = -L_{orb}^{+}$, and $L_{orb} = 0$. In the next section we present a case study where we analyze the L_{orb}^{\pm} terms of a Brewster-reflected paraxial beam-field; and thus explore their significant contribution in characterizing the SOI phenomenon.

III. CASE STUDY : SPIN-ORBIT INTERACTION IN A BREWSTER-REFLECTED PARAXIAL BEAM

In our earlier work of Ref. [65] we have described an optical system, where an initial collimated beam with

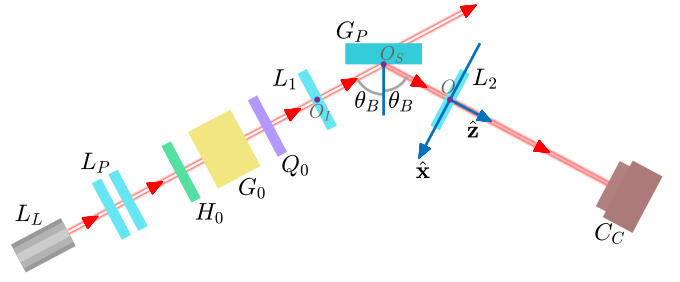


FIG. 1. The Brewster-reflection experimental setup, with a He-Ne laser source L_L , collimating lens-pair L_P , half wave plate (HWP) H_0 , Glan-Thompson polarizer (GTP) G_0 , quarter wave plate (QWP) Q_0 , diverging lens L_1 , collimating lens L_2 , glass plate G_P to set a reflecting surface, and CCD camera C_C for observation.

uniform polarization is diverged through a lens, and subsequently reflected at a plane dielectric interface, with the central angle of incidence being the Brewster angle θ_B [Fig. 1]. The reflected diverging beam is collimated and observed at a screen (CCD camera). The output field profile obtained at the screen has the form

$$\mathcal{E} = \mathcal{E}^X + e^{i\Phi_E} \mathcal{E}^Y; \quad (13)$$

where, \mathcal{E}^X and \mathcal{E}^Y are output fields corresponding to the individual \hat{x} -polarized and \hat{y} -polarized input fields; and Φ_E is their phase difference. In particular, if the input field is purely \hat{x} -polarized, then we get only $\mathcal{E} = \mathcal{E}^X$, which can be straightforwardly expressed in the form of Eq. (1) by defining (first order approximation)

$$\mathcal{E}_x = A_1(x/w_R)G_R; \quad \mathcal{E}_y = A_2(y/w_R)G_R; \quad (14)$$

where, A_1 and A_2 are field amplitude terms; w_R is the effective half-width of the output collimated beam; and $G_R = e^{-\rho^2/w_R^2}$ ($\rho = \sqrt{x^2 + y^2}$) represents an overall Gaussian envelope. The field functions \mathcal{E}_x and \mathcal{E}_y are thus first order Hermite-Gaussian (HG) modes.

Using Eq. (14) in Eqs. (2) and (3), we obtain $M_{spin} = M_{orb} = 0$; which, via Eq. (4), gives $L_{spin} = L_{orb} = 0$. Zero SAM and OAM of the total field \mathcal{E} is thus interpreted from this straightforward L_{spin} and L_{orb} calculation — where the true nature of SOI remains unexpressed.

To explore this nature we now analyze the individual \mathcal{E}_{\pm} component fields. Using Eq. (14) in Eq. (6), we obtain

$$\mathcal{E}_{\pm} = (G_R/\sqrt{2}w_R) (A_1x \mp iA_2y) = \mathcal{E}_0 e^{i\Phi_{\pm}}; \quad (15a)$$

$$\mathcal{E}_0 = (G_R/\sqrt{2}w_R) (A_1^2x^2 + A_2^2y^2)^{\frac{1}{2}}; \quad (15b)$$

$$\Phi_{\pm} = \mp \tan^{-1}[(A_2/A_1) \tan \phi]; \quad (15c)$$

where, ϕ is the azimuthal coordinate. The total field \mathcal{E} is then expressed by using Eqs. (6) as

$$\mathcal{E} = \mathcal{E}_0 (e^{i\Phi_+} \hat{\sigma}^+ + e^{i\Phi_-} \hat{\sigma}^-). \quad (16)$$

This is a non-separable state that describes a coupling between the spatial and polarization states. Since the OAM information is contained in the spatial states, and the $\hat{\sigma}^\pm$ polarizations are spin states, Eq. (16) expresses the true nature of SOI in the field \mathcal{E} — indicating towards the distribution of OAM between the $\hat{\sigma}^\pm$ spin-component fields. Clearly, at the origin, $\mathcal{E}_0 = 0$ and Φ_\pm are singular [65]. The topological charges of the phases Φ_\pm , which are defined in the form [36, 37, 66, 67]

$$t = \frac{1}{2\pi} \oint_C \nabla \Phi(\mathbf{r}) \cdot d\mathbf{r}, \quad (17)$$

are obtained here as $t_\pm = \mp 1$ — physically signifying that, if ϕ is increased by 2π , the phases Φ_\pm change by $\mp 2\pi$. However, here Φ_\pm are not proportional to ϕ . One would obtain $\Phi_\pm = \mp \phi$ for a case of $A_1 = A_2$, which would identify \mathcal{E}_\pm as pure Laguerre-Gaussian modes with $l = \mp 1$. However, for the presently considered Brewster-reflection case, we have $A_1 \neq A_2$ [65] — giving rise to complicated ϕ -dependencies of Φ_\pm via Eq. (15c). The Φ_\pm phase vortices of complicated ϕ -dependencies are thus non-canonical phase vortices [36] with topological charges $t_\pm = \mp 1$.

Using Eq. (15a) in Eq. (8), we now obtain the OAM flux densities of the \mathcal{E}_\pm component fields as

$$M_{orb}^\pm = \mp \frac{\epsilon_0}{2k} \frac{A_1 A_2}{2} \frac{\rho^2}{w_R^2} G_R^2. \quad (18)$$

Using this in Eq. (9), we obtain the OAM fluxes

$$L_{orb}^\pm = \mp \frac{\epsilon_0}{2k} A_1 A_2 \frac{\pi w_R^2}{8}. \quad (19)$$

The distribution of OAM between the \mathcal{E}_\pm fields is exactly quantified by this result. Clearly, $L_{orb}^- = -L_{orb}^+$; which is consistent with the total OAM flux $L_{orb} = 0$ (OAM conservation). Also, it is easily verified by using Eqs. (9) and (18) that L_{orb}^\pm are independent of the coordinate system — ensuring L_{orb}^\pm to represent the intrinsic OAM fluxes. A special-case result of the SOI phenomenon of distribution of OAM, as interpreted in the present paper, is thus expressed by Eq. (19).

To obtain an equivalent single-photon interpretation, we first obtain the powers of the \mathcal{E}_\pm fields by using Eq. (15a) as

$$P_\pm = \frac{1}{2\mu_0 c} \int_{-\infty}^{\infty} \int_{-\infty}^{\infty} |\mathcal{E}_\pm|^2 dx dy = \frac{1}{2\mu_0 c} \frac{A_1^2 + A_2^2}{2} \frac{\pi w_R^2}{8}. \quad (20)$$

The OAM per photon corresponding to \mathcal{E}_\pm are then obtained as

$$l_{orb}^\pm = (L_{orb}^\pm / P_\pm) \hbar \omega = \mp \frac{2A_1 A_2}{A_1^2 + A_2^2} \hbar. \quad (21)$$

Thus, in the total beam-field \mathcal{E} , a photon with spin $\hat{\sigma}^\pm$ carries an OAM l_{orb}^\pm given by Eq. (21). These l_{orb}^\pm OAM are fractions of $\mp \hbar$, since $A_1 \neq A_2$. These fractional

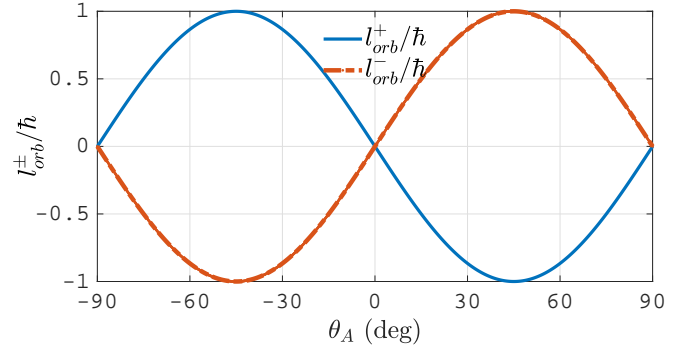


FIG. 2. Variation of l_{orb}^\pm with respect to θ_A [Eq. (23)]. The variation of θ_A signifies different contributions of \mathcal{E}_x and \mathcal{E}_y [Eq. (14)] in the total field \mathcal{E} .

OAM are unrelated to any fractional vortex [17, 26], because the topological charges of the presently considered vortices are $t^\pm = \mp 1$. Instead, these are related to the non-canonical nature [36] of the vortices of the phases Φ_\pm [Eq. (15c)].

To understand the dependence of l_{orb}^\pm on the field amplitudes A_1 and A_2 , we express A_1 and A_2 in terms of a parameter θ_A as

$$A_1 = A_0 \cos \theta_A, \quad A_2 = A_0 \sin \theta_A, \quad (22)$$

where A_0 is an overall amplitude term. The variation of θ_A determines the contributions of \hat{x} and \hat{y} polarized components to the total field \mathcal{E} via Eqs. (14) and (22). Using Eq. (22) in Eq. (21), l_{orb}^\pm can be re-expressed as

$$l_{orb}^\pm = \mp (\sin 2\theta_A) \hbar. \quad (23)$$

The variation of l_{orb}^\pm with respect to θ_A is shown in Fig. 2. For $\theta_A = 0^\circ, \pm 90^\circ$, either \mathcal{E}_x or \mathcal{E}_y is non-zero. The total field \mathcal{E} is thus in a pure HG mode; and according to Eq. (23) [Fig. 2], the component \mathcal{E}_\pm fields do not possess any OAM. For $\theta_A = \pm 45^\circ$, both \mathcal{E}_x and \mathcal{E}_y have equal amplitude moduli $|A_1| = |A_2|$. The component \mathcal{E}_\pm fields are then in pure LG modes, having OAM per photon $\mp \hbar$ or $\pm \hbar$. For other values of θ_A , other values of the ratio A_2/A_1 are obtained, and the OAM per photon of the \mathcal{E}_\pm fields vary according to the graph of Fig. 2 — while satisfying the relation $l_{orb}^- = -l_{orb}^+$ for all θ_A . For the Brewster reflection case in particular [65], A_2/A_1 is obtained in the range $0 < A_2/A_1 < 1$. Consequently, l_{orb}^\pm are obtained as fractions of $\mp \hbar$ according to Eqs. (21) and (23) [Fig. 2].

The non-separable state representation of Eq. (16) can also be interpreted in terms of the above single-photon picture. The non-separable state implies that, if a single photon is detected in a polarization state $\hat{\sigma}^\pm$, it is also readily identified to be in a spatial state $\mathcal{E}_\pm = \mathcal{E}_0 e^{i\Phi_\pm}$. To verify that the spatial states \mathcal{E}_\pm indeed carry OAM l_{orb}^\pm given by Eq. (21) (without involving a classical OAM

flux calculation, Eqs. (18)–(21)); we re-express \mathcal{E}_\pm [Eq. (15a)] as (using $x = \rho \cos \phi$, $y = \rho \sin \phi$)

$$\mathcal{E}_\pm = (\rho G_R / \sqrt{2} w_R) (B_1 e^{\mp i \phi} + B_2 e^{\pm i \phi}); \quad (24a)$$

$$B_1 = (A_1 + A_2)/2, \quad B_2 = (A_1 - A_2)/2. \quad (24b)$$

The states \mathcal{E}_\pm are thus linear combinations of pure LG modes with $l = \pm 1$, with coefficient amplitude terms B_1 and B_2 . The LG modes with $l = \pm 1$ have OAM per photon $\pm \hbar$. The expectation values of the OAM per photon associated to the \mathcal{E}_\pm states are then obtained as

$$l_{orb}^\pm = \frac{B_1^2(\mp \hbar) + B_2^2(\pm \hbar)}{B_1^2 + B_2^2} = \mp \frac{2A_1 A_2}{A_1^2 + A_2^2} \hbar; \quad (25)$$

which is the same result as in Eq. (21). In this way the fractional OAM l_{orb}^\pm is explained from the single-photon picture. Hence, if a photon is detected in a polarization state $\hat{\sigma}^\pm$, it is readily identified to carry an OAM l_{orb}^\pm — while the average OAM per photon of the complete non-separable field-state \mathcal{E} is $(l_{orb}^+ + l_{orb}^-)/2 = 0$, satisfying OAM conservation.

The calculation of l_{orb}^\pm via Eq. (25) is equivalent to Berry's calculation of average OAM per photon [16]. As explained by Berry, a phase vortex of topological charge t is not necessarily associated to an OAM $t\hbar$ per photon, unless the state is a pure LG mode with $l = t$ — which is equivalent to the canonical/non-canonical vortex interpretation. The Brewster reflection case considered in the present paper clearly presents a significant example of this interpretation.

IV. GEOMETRIC PHASE CHARACTERISTICS

A. Interpretation

It may appear paradoxical that, in the above analysis, the SOI phenomena are observed in a collimated beam without considering any wavefront curvature. But the resolution lies in the fact that the SOI truly occurs at the dielectric interface, where the spherically diverging wavefront is reflected. A formal SOI analysis at the interface can be carried out by expressing the diverging beam-field in the momentum space in terms of helicity basis states, via which the SOI can be seamlessly interpreted as a manifestation of the inherent geometric phase characteristics of the field [33, 36]. Instead, in the present analysis, we transform the reflected diverging beam to a collimated beam and determine the SAM and OAM flux densities — thus extracting the same SOI information in a different way by involving Barnett's formulation [25].

Nevertheless, the involvement of geometric phase in the present analysis is clearly understood by considering the equivalence of the variable phases Φ_\pm with geometric phase (see, e.g., Ref. [33] for a detailed review). The component fields \mathcal{E}_\pm , expressed in the form $\mathcal{E}_\pm = \mathcal{E}_0 e^{i\Phi_\pm} \hat{\sigma}^\pm$,

are comparable to Berry's Eq. (5) of Ref. [68]:

$$|\psi(T)\rangle = \exp(i\gamma_n(C)) \exp \left\{ \frac{-i}{\hbar} \int_0^T dt E_n(\mathbf{R}(t)) \right\} |\psi(0)\rangle. \quad (26)$$

In this comparison, the polarization states $\hat{\sigma}^\pm$ are comparable to the primary state $|\psi(0)\rangle$; the suppressed time-dependence term $e^{-i\omega t}$ is comparable to the time-dependence term $\exp \left\{ (-i/\hbar) \int_0^T dt E_n(\mathbf{R}(t)) \right\}$; and the phase variation term $e^{i\Phi_\pm}$ is comparable to the geometric phase dependence term $\exp(i\gamma_n(C))$. By following Pancharatnam's formulation [69], we can then interpret that the fields $\mathcal{E}_\pm = \mathcal{E}_0 e^{i\Phi_\pm} \hat{\sigma}^\pm$ are $\hat{\sigma}^\pm$ -polarized everywhere at the beam cross-section; but at different spatial points the $\hat{\sigma}^\pm$ polarizations are reached from different equatorial points of the Poincaré sphere — giving rise to the 'overall' variable phases Φ_\pm . The spatially varying Φ_\pm phases are thus interpreted as geometric phases. Hence, the SOI phenomena in the present formalism are indeed associated to the inherent geometric phase characteristics of the beam-field — as is the case for the curved-wavefront-based formulations [33, 36].

The geometric phase characteristics discussed above are associated to the fundamental polarization inhomogeneity of the beam-field. Interpreted in terms of Eqs. (15), the spatially varying field functions \mathcal{E}_\pm give rise to the geometric phases Φ_\pm , which in turn cause the SOI. Whereas, interpreted in terms of Eq. (8), the field functions \mathcal{E}_\pm give rise to non-zero OAM flux densities M_{orb}^\pm , which cause the considered OAM distribution between the spin-component fields. The equivalence between the inhomogeneous polarization description and the geometric phase description is thus established — which give rise to the same SOI phenomenon. Though we describe this equivalence in the context of a Brewster reflection analysis, an inhomogeneously polarized beam-field can originate from many physical processes, including reflection and transmission at dielectric interfaces [4, 27–31, 40–63]. The above-mentioned equivalence between this inhomogeneous polarization and geometric phase can be easily established in all such cases.

B. Experimental Measurement of Geometric Phase

For a field of the form $\mathcal{E}_\pm = \mathcal{E}_0 e^{i\Phi_\pm} \hat{\sigma}^\pm$, a direct experimental measurement of the geometric phase Φ_\pm is not physically realizable. A measurement of the phase Φ_{23} of the complex Stokes parameter $S_2 + iS_3$ [70] gives only the phase difference between the \hat{x} and \hat{y} components, which is simply $\pm\pi/2$ for $\hat{\sigma}^\pm$. A widely used method for identifying a variable phase structure is to superpose it with a coherent plane-wave beam and to observe the interference pattern [9, 13, 14]. However, a plane-wave beam coherent with the source of the beam under examination may not be available in all cases, which limits the applicability of this method. Another identification method

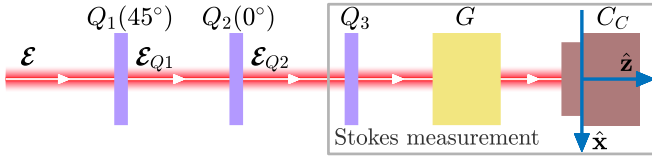


FIG. 3. Transfer of geometric phase information to polarization domain; and the subsequent Stokes measurement. Here, Q_1 , Q_2 , Q_3 are QWPs; G is GTP; CC is CCD camera; and \mathcal{E} is the final output beam-field after the lens L_2 in the setup of Fig. 1. It is to be noticed that, to capture the relevant Stokes measurement images involving Q_3 , the fast axis of Q_3 must be oriented along \hat{y} ; which is equivalent to removing Q_2 whose fast axis is oriented along \hat{x} . The experiment can thus be practically performed without using Q_3 at all.

specifically for a vortex phase structure is the generation of its single-slit diffraction pattern, by observing which the topological charge t of the vortex can be identified [71]. However, identification of the charge t is not sufficient to identify the true phase structure, because the vortex can in general be non-canonical [16, 36].

However, SOI in the complete beam-field \mathcal{E} expressed in the form of Eq. (16) enables a partial extraction of the geometric phase information in all general cases, and a complete measurement of it in a specific subset of special cases — without using any reference plane wave coherent with the source, and without the ambiguity present in the single-slit diffraction observations. In this subsection we first develop our experimental method by considering a general form of the field \mathcal{E} as

$$\mathcal{E} = \mathcal{E}_{0+} e^{i\Phi_+} \hat{\sigma}^+ + \mathcal{E}_{0-} e^{i\Phi_-} \hat{\sigma}^-; \quad (27)$$

for which no specially derived form involving Eqs. (1), (6), (13)–(15) is assumed. After developing a partial information extraction scheme for this general case, we consider a special case of Eq. (1), for which we extract the complete information.

In the first stage we aim to measure the geometric phase difference $\Delta\Phi = \Phi_- - \Phi_+$, which itself is a variable phase term over the entire beam cross-section. For this purpose, we first pass the beam-field \mathcal{E} (which, for our purpose, is the collimated output beam-field after the lens L_2 in the setup of Fig. 1) through a quarter wave plate (QWP) Q_1 [Fig. 3], whose fast axis is oriented along $\hat{d}^+ = (\hat{x} + \hat{y})/\sqrt{2}$. Due to this, the polarizations $\hat{\sigma}^+$ and $\hat{\sigma}^-$ transform respectively to $e^{-i\pi/4} \hat{x}$ and $-e^{i\pi/4} \hat{y}$. Here, the $\pm\pi/4$ phase terms are additional geometric phases which are introduced due to the coordinate system rotation associated to the rotated QWP operation. The complete field \mathcal{E} is thus transformed to

$$\begin{aligned} \mathcal{E}_{Q1} &= \mathcal{E}_{0+} e^{i\Phi_+} e^{-i\pi/4} \hat{x} - \mathcal{E}_{0-} e^{i\Phi_-} e^{i\pi/4} \hat{y} \\ &= e^{i\Phi_+} e^{-i\pi/4} \left(\mathcal{E}_{0+} \hat{x} + \mathcal{E}_{0-} e^{i\Delta\Phi} e^{-i\pi/2} \hat{y} \right). \end{aligned} \quad (28)$$

We now pass this beam-field \mathcal{E}_{Q1} through a second QWP Q_2 , whose fast axis is oriented along \hat{x} . This eliminates

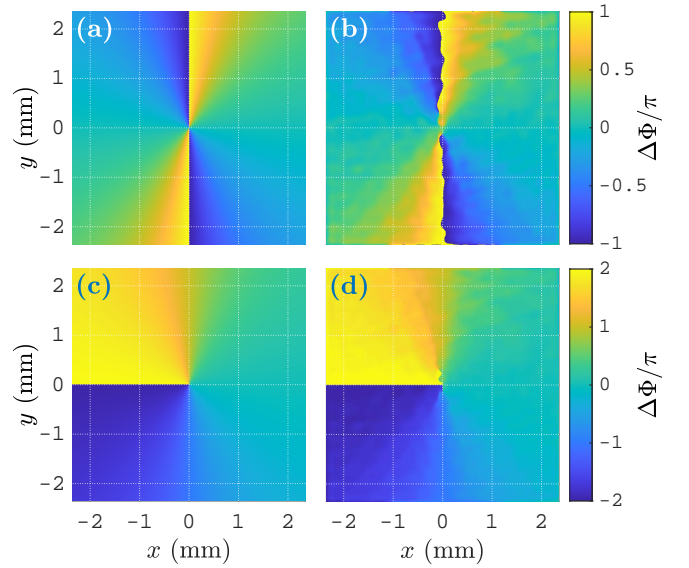


FIG. 4. Geometric phase difference $\Delta\Phi = \Phi_- - \Phi_+$ at the beam cross section: (a) simulated and (b) experimental, expressed in range $(-\pi, \pi]$; (c) simulated and (d) experimental, expressed in range $(-2\pi, 2\pi]$.

the relative phase $-\pi/2$ associated to the \hat{y} component, and transforms the field \mathcal{E}_{Q1} to

$$\mathcal{E}_{Q2} = e^{i\Phi_+} e^{-i\pi/4} (\mathcal{E}_{0+} \hat{x} + \mathcal{E}_{0-} e^{i\Delta\Phi} \hat{y}). \quad (29)$$

The geometric phase difference $\Delta\Phi$ is thus transformed to the phase-lead of the \hat{y} component with respect to the \hat{x} component of \mathcal{E}_{Q2} , and can be straightforwardly measured in the form of the phase Φ_{23} of the complex Stokes parameter $S_2 + iS_3$.

For the simulation and experiment, we consider the following parameter values in the setup of Fig. 1: refractive indices $n_1 = 1$, $n_2 = 1.52$; laser power 1 mW, free-space wavelength $\lambda = 632.8$ nm; input beam half-width $w_0 = 0.8$ mm; focal length of lens $L_1 = -5$ cm, focal length of lens $L_2 = 12.5$ cm; propagation path-lengths $O_I O_S = 5$ cm, $O_S O_R = 2.5$ cm. The simulated and experimentally generated profiles of $\Delta\Phi$ are shown in Fig. 4, showing agreement between the two results. An experimental geometric phase difference measurement is thus achieved by using the above method.

Since the above method is established based only on the general expression of Eq. (27) without assuming any special form of the beam-field, it is applicable seamlessly to all paraxial beams. The observed $\Delta\Phi$ profile, however, gives partial information on the geometric phases, because the Φ_{\pm} phases are not measured individually. As understood from the derivation of Eq. (29), either Φ_+ or Φ_- can be separated as an overall phase term, and hence its direct measurement is a physical impossibility. At this premise we now proceed towards the second stage of the computation, where we consider a special case of Eq. (1)

that both \mathcal{E}_x and \mathcal{E}_y are real. Any locally linearly polarized beam-field, irrespective of any non-uniformity of the polarization directions over the beam cross-section, can be expressed in this form. The presently considered Brewster-reflected beam-field can be considered as an example, because, according to Eq. (14), both \mathcal{E}_x and \mathcal{E}_y are real everywhere. The phases Φ_{\pm} are then determined by using Eq. (6) as $\Phi_{\pm} = \mp \tan^{-1}(\mathcal{E}_y/\mathcal{E}_x)$; so that a relation $\Phi_+ + \Phi_- = 0$ is satisfied. Considering this along with the relation $\Delta\Phi = \Phi_- - \Phi_+$, we obtain the individual phases

$$\Phi_{\pm} = \mp \Delta\Phi/2. \quad (30)$$

Figures 5(a) and 5(b) show the plots of Φ_{\pm} by using the expressions of Eq. (15c) for the presently considered simulated system. Figures 5(c) and 5(d) show the plots of Φ_{\pm} by considering Eq. (30), using the experimentally obtained $\Delta\Phi$ data of Fig. 4(d). The simulated and experimental results match well, thus validating our phase determination method.

In this way, a direct measurement method for geometric phase is established by using appropriate transformations and subsequent Stokes parameter measurements — which is another central content of the present paper. One may qualitatively visualize that, since spin characteristics and orbital characteristics are coupled in the system, we have made use of this interaction to transfer orbital/spatial information to the spin/polarization domain; so that subsequently the information is extracted via polarization measurements. From this perspective, our experimental method is comparable to a quantum mechanical measurement process. In a von Neumann measurement [64], a coupled state of a measurand system and a measuring device is created, so that the information on the measurand system state can be extracted by observing the measuring device state. In our experiment, the spatial parts of the field function (which contain the OAM information) are comparable to measurand system states; whereas, the polarization states are comparable to measuring device states. Our geometric phase measurement method is thus a classical analog of quantum mechanical von Neumann measurement. In this way, at the core of the effectiveness of our experimental method, there exists SOI.

The special case consideration of our method also shows that real \mathcal{E}_x and \mathcal{E}_y in Eq. (1) lead to the relation $\Phi_+ + \Phi_- = 0$ between the geometric phases. Also, by using real \mathcal{E}_x and \mathcal{E}_y (irrespective of their functional forms) in Eq. (3), we obtain $M_{orb} = 0$; which, via Eq. (11), leads to $M_{orb}^+ + M_{orb}^- = 0$. The relations $\Phi_+ + \Phi_- = 0$ and $M_{orb}^+ + M_{orb}^- = 0$ are thus equivalent — one represented in terms of geometric phases and the other represented in terms of OAM flux densities — representing a special nature of SOI for locally linearly polarized fields. An additional method of experimental verification of the above nature, specifically for the presently considered vortex phases, is the observation of topological charges via single-slit diffraction patterns. We pass

the complete beam-field \mathcal{E} (or equivalently, the field \mathcal{E}_{Q2} , Eq. (29)) through a single vertical slit of width 0.5 mm, placed along $x = 0$. Though a decreased intensity in the diffraction pattern is observed around the central dark region of the beam-field, no fringe-dislocation is observed [Fig. 6(a)] — implying that the topological charge of the complete beam-field is zero. We subsequently pass the \hat{x} and \hat{y} polarized component fields of \mathcal{E}_{Q2} —

$$\mathcal{E}_{Q2x} = \mathcal{E}_{0+} e^{i\Phi_+} e^{-i\pi/4} \hat{x} \quad \text{and} \quad \mathcal{E}_{Q2y} = \mathcal{E}_{0-} e^{i\Phi_-} e^{-i\pi/4} \hat{y} \quad (31)$$

— through the same slit, by extracting them individually with appropriate orientations of a GTP. The diffraction patterns corresponding to \mathcal{E}_{Q2x} and \mathcal{E}_{Q2y} show appropriate opposite fringe-dislocations [Figs. 6(b) and 6(c)], which are signatures of topological charges -1 and $+1$ respectively. This observation verifies that, even if the complete field \mathcal{E} does not carry any topological charge, the spin-polarized component fields \mathcal{E}_{\pm} with phase profiles Φ_{\pm} carry topological charges $t_{\pm} = \mp 1$.

C. Comments on Beam-shifts and Spin-shifts

Finally, the SOI is in general expected to cause beam-shifts and spin-shifts. Considering the intensity profiles $I = (n_1/2\mu_0c)|\mathcal{E}|^2$ and $I_{\pm} = (n_1/2\mu_0c)|\mathcal{E}_{\pm}|^2$ of the fields \mathcal{E} and \mathcal{E}_{\pm} , the GH and IF shifts [4, 27, 28, 40–54] are obtained as the longitudinal (along x) and transverse (along y) shifts of the I centroid from the origin; whereas, the longitudinal and transverse spin-shifts [55–62] are obtained as the longitudinal and transverse shifts of the I_{\pm} centroids from the origin. However, for the considered special case of Brewster reflection, the special forms of \mathcal{E}_x and \mathcal{E}_y [Eq. (14)] place all the above centroids at the origin — thus resulting in zero beam-shifts and zero spin-shifts. Hence, even though beam-shifts and spin-shifts are sufficient signatures of SOI, they are not necessarily its definite outcomes. The presently considered Brewster reflection case is an example, where SOI causes a distribution of OAM among the spin-component fields without shifting the beam-centroid and spin-centroid positions.

V. CONCLUSION

In the present paper, we have interpreted that the OAM of a complete paraxial beam-field is consistently distributed between its spin-polarized component beam-fields — which is a subtle and fundamental nature of SOI in the beam-field. We have used Barnett's formalism of calculating SAM and OAM fluxes to derive a general formula expressing the individual OAM flux distributions of the spin-component fields, and hence have verified that AM conservation is satisfied in this distribution mechanism. Then we have considered a case study involving the Brewster reflection of a paraxial beam, and have explored the OAM characteristics of its spin-polarized com-

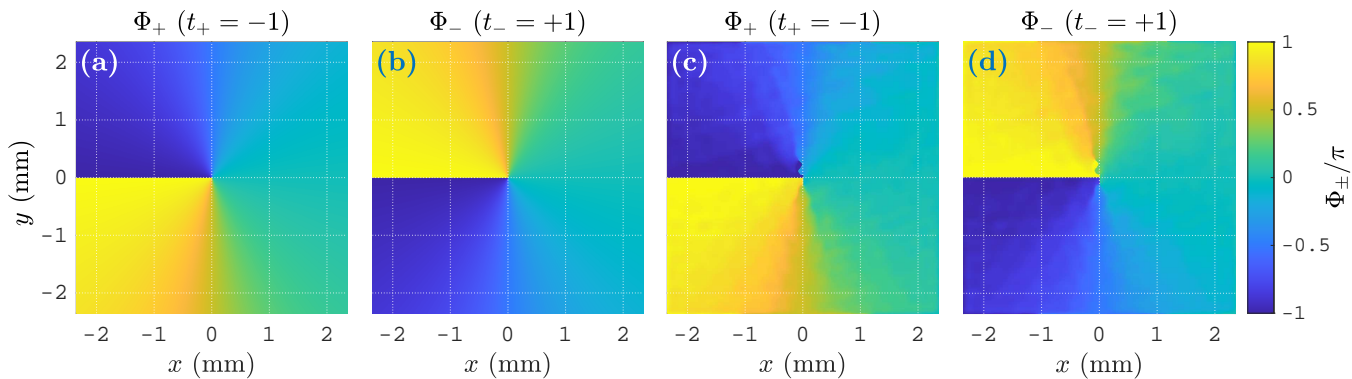


FIG. 5. Geometric phase profiles Φ_{\pm} , showing topological charges $t_{\pm} = \mp 1$: (a), (b) simulated; (c), (d) experimental.

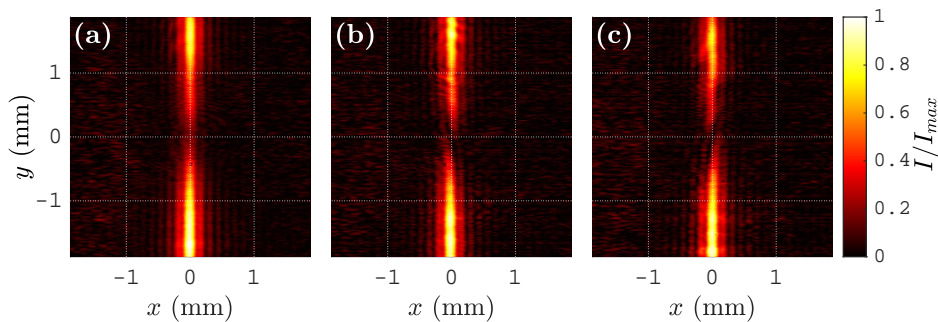


FIG. 6. Single-slit diffraction patterns generated by the beam-fields (a) \mathcal{E} [Eq. (27)], showing no fringe-dislocation; (b) \mathcal{E}_{Q2x} [Eq. (31)], showing fringe-dislocation for topological charge $t = -1$; (c) \mathcal{E}_{Q2y} [Eq. (31)], showing fringe-dislocation for topological charge $t = +1$.

ponent fields. Consideration of this special case is particularly important, because the spin-component fields here contain phase vortices giving rise to fundamentally interesting special properties, such as non-canonical vortex nature — which we have explored here in detail. In addition to the classical flux calculations, we have also explored an equivalent single-photon picture of the beam-field, by interpreting the spin-orbit-coupled field function as a non-separable photon state.

The phase structures of the spin-component beam-fields are equivalent to geometric phases — an interpretation which we have explored subsequently. We have devised an experimental method, by which the geometric phase difference is transformed to a phase difference between the \hat{x} and \hat{y} component fields — so that it can be directly observed via Stokes parameter measurements. Thus, we have made use of the SOI of the beam field to transfer the spatial phase information to the polariza-

tion domain — a process which can be interpreted as a classical analog of quantum mechanical von Neumann measurements.

To summarize, our formalism explores fundamental details on the SOI in a general paraxial beam-field by mathematically characterizing its OAM distribution; whereas, our experimental geometric phase measurement method achieves a convenient way of transferring orbital information to spin domain by utilizing the SOI. We anticipate that such a direct geometric phase measurement method can be significantly upgraded in the future and be efficiently applied to paraxial as well as non-paraxial beam-fields.

ACKNOWLEDGMENTS

A.D. thanks CSIR for Senior Research Fellowship. N.K.V. thanks SERB for financial support.

[1] J. H. Poynting, Proc. R. Soc. A **82**, 560 (1909).

[2] R. A. Beth, Phys. Rev. **50**, 115 (1936).

- [3] L. Allen, M. W. Beijersbergen, R. J. C. Spreeuw, and J. P. Woerdman, *Phys. Rev. A* **45**, 8185 (1992).
- [4] V. S. Liberman and B. Y. Zel'dovich, *Phys. Rev. A* **46**, 5199 (1992).
- [5] S. J. van Enk and G. Nienhuis, *Opt. Commun.* **94**, 147 (1992).
- [6] G. Nienhuis and L. Allen, *Phys. Rev. A* **48**, 656 (1993).
- [7] S. J. van Enk and G. Nienhuis, *Europhys. Letts.* **25**, 497 (1994).
- [8] S. M. Barnett and L. Allen, *Opt. Commun.* **110**, 670 (1994).
- [9] M. Harris, C. A. Hill, and J. M. Vaughan, *Opt. Commun.* **106**, 161 (1994).
- [10] M. W. Beijersbergen, R. P. C. Coerwinkel, M. Kristensen, and J. P. Woerdman, *Opt. Commun.* **112**, 321 (1994).
- [11] H. He, M. E. J. Friese, N. R. Heckenberg, and H. Rubinsztein-Dunlop, *Phys. Rev. Lett.* **75**, 826 (1995).
- [12] M. E. J. Friese, J. Enger, H. Rubinsztein-Dunlop, and N. R. Heckenberg, *Phys. Rev. A* **54**, 1593 (1996).
- [13] M. Padgett, J. Arlt, N. Simpson, and L. Allen, *Am. J. Phys.* **64**, 77 (1996).
- [14] M. S. Soskin, V. N. Gorshkov, M. V. Vasnetsov, J. T. Malos, and N. R. Heckenberg, *Phys. Rev. A* **56**, 4064 (1997).
- [15] R. Bhandari, *Phys. Rep.* **281**, 1 (1997).
- [16] M. V. Berry, in *Proc. SPIE*, Vol. 3487 (1998) pp. 6–11.
- [17] M. V. Vasnetsov, I. V. Basistiy, and M. S. Soskin, in *International Conference on Singular Optics*, Vol. 3487, edited by M. S. Soskin, International Society for Optics and Photonics (SPIE, 1998) pp. 29–33.
- [18] L. Allen, J. Courtial, and M. J. Padgett, *Phys. Rev. E* **60**, 7497 (1999).
- [19] L. Allen and M. J. Padgett, *Opt. Commun.* **184**, 67 (2000).
- [20] M. Padgett and A. Allen, *Contemp. Phys.* **41**, 275 (2000).
- [21] A. Mair, A. Vaziri, G. Weihs, and A. Zeilinger, *Nature* **412**, 313 (2001).
- [22] G. Molina-Terriza, J. Recolons, J. P. Torres, L. Torner, and E. M. Wright, *Phys. Rev. Lett.* **87**, 023902 (2001).
- [23] M. J. Padgett and L. Allen, *J. Opt. B* **4**, S17 (2002).
- [24] A. T. O'Neil, I. MacVicar, L. Allen, and M. J. Padgett, *Phys. Rev. Lett.* **88**, 053601 (2002).
- [25] S. M. Barnett, *J. Opt. B* **4**, S7 (2002).
- [26] M. V. Berry, *J. Opt. A* **6**, 259 (2004).
- [27] M. Onoda, S. Murakami, and N. Nagaosa, *Phys. Rev. Lett.* **93**, 083901 (2004).
- [28] O. Hosten and P. Kwiat, *Science* **319**, 787 (2008).
- [29] K. Y. Bliokh, Y. Gorodetski, V. Kleiner, and E. Hasman, *Phys. Rev. Lett.* **101**, 030404 (2008).
- [30] K. Y. Bliokh, *J. Opt. A: Pure Appl. Opt.* **11**, 094009 (2009).
- [31] K. Y. Bliokh, M. A. Alonso, E. A. Ostrovskaya, and A. Aiello, *Phys. Rev. A* **82**, 063825 (2010).
- [32] K. Y. Bliokh and F. Nori, *Phys. Rep.* **592**, 1 (2015).
- [33] K. Y. Bliokh, M. A. Alonso, and M. R. Dennis, *Rep. Prog. Phys.* **82**, 122401 (2019).
- [34] M. V. Berry and P. Shukla, *J. Opt.* **21**, 064002 (2019).
- [35] L. Allen, S. M. Barnett, and M. J. Padgett, eds., *Optical Angular Momentum* (Institute of Physics Publishing, Bristol and Philadelphia, 2003).
- [36] D. L. Andrews and M. Babiker, eds., *The Angular Momentum of Light* (Cambridge University Press, Cambridge, UK, 2013).
- [37] G. J. Gbur, *Singular Optics* (CRC Press, Taylor & Francis Group, LLC, FL, 2017).
- [38] M. S. Soskin and M. V. Vasnetsov, *Prog. Opt.* **42**, 219 (2001).
- [39] M. R. Dennis, K. O'Holleran, and M. J. Padgett, *Prog. Opt.* **53**, 293 (2009).
- [40] V. F. Goos and H. Hänchen, *Ann. Physik* **436**, 333 (1947).
- [41] K. Artmann, *Ann. Physik* **437**, 87 (1948).
- [42] J. W. Ra, H. L. Bertoni, and L. B. Felsen, *SIAM J. Appl. Math.* **24**, 396 (1973).
- [43] Y. M. Antar and W. M. Boerner, *Can. J. Phys.* **52**, 962 (1974).
- [44] M. McGuirk and C. K. Carniglia, *J. Opt. Soc. Am.* **67**, 103 (1977).
- [45] C. C. Chan and C. Tamir, *Opt. Lett.* **10**, 378 (1985).
- [46] M. A. Porras, *Optics Communications* **131**, 13 (1996).
- [47] A. Aiello and J. P. Woerdman, arXiv:0903.3730v2 [physics.optics] (2009).
- [48] F. I. Fedorov, *Dokl. Akad. Nauk SSSR* **105**, 465 (1955), english translation available at <http://master.basnet.by/congress2011/symposium/spbi.pdf>.
- [49] H. Schilling, *Ann. Physik* **471**, 122 (1965).
- [50] C. Imbert, *Phys. Rev. D* **5**, 787 (1972).
- [51] M. A. Player, *J. Phys. A: Math. Gen.* **20**, 3667 (1987).
- [52] V. G. Fedoseyev, *J. Phys. A: Math. Gen.* **21**, 2045 (1988).
- [53] K. Y. Bliokh and Y. P. Bliokh, *Phys. Rev. Lett.* **96**, 073903 (2006).
- [54] K. Y. Bliokh and Y. P. Bliokh, *Phys. Rev. E* **75**, 066609 (2007).
- [55] A. Aiello and J. P. Woerdman, arXiv:0710.1643v2 [physics.optics] (2007).
- [56] A. Aiello and J. P. Woerdman, *Opt. Lett.* **33**, 1437 (2008).
- [57] M. Merano, A. Aiello, M. P. van Exter, and J. P. Woerdman, *Nature Photon* **3**, 337 (2009).
- [58] A. Aiello, M. Merano, and J. P. Woerdman, *Phys. Rev. A* **80**, 061801(R) (2009).
- [59] Y. Qin, Y. Li, X. Feng, Y.-F. Xiao, H. Yang, and Q. Gong, *Opt. Express* **19**, 9636 (2011).
- [60] K. Y. Bliokh and A. Aiello, *J. Opt.* **15**, 014001 (2013).
- [61] J. B. Götte, W. Löffler, and M. R. Dennis, *Phys. Rev. Lett.* **112**, 233901 (2014).
- [62] L. Xie, X. Zhou, X. Qiu, L. Luo, X. Liu, Z. Li, Y. He, J. Du, Z. Zhang, and D. Wang, *Opt. Express* **26**, 22934 (2018).
- [63] A. Debnath and N. K. Viswanathan, *J. Opt. Soc. Am. A* **37**, 1971 (2020).
- [64] J. von Neumann, *Mathematical Foundations of Quantum Mechanics* (Princeton University Press, Princeton, 1955).
- [65] A. Debnath and N. K. Viswanathan, *Phys. Rev. A* **103**, 013510 (2021).
- [66] J. F. Nye and M. V. Berry, *Proc. R. Soc. Lond. A* **336**, 165 (1974).
- [67] M. V. Berry and J. H. Hannay, *J. Phys. A: Math. Gen.* **10**, 1809 (1977).
- [68] M. V. Berry, *Proc. R. Soc. A* **392**, 45 (1984).
- [69] S. Pancharatnam, *Proc. Ind. Acad. Sci. A* **44**, 247 (1956).
- [70] D. H. Goldstein, *Polarized Light*, 3rd ed. (CRC Press, Taylor & Francis Group, FL, 2011).
- [71] D. P. Ghai, P. Senthikumar, and R. S. Sirohi, *Opt Laser Eng* **47**, 123 (2009).